Taking into account that $j = x^{n/2}$ and $x^n = -1$ in evaluating eqns. 6 and 9, the coefficients c_i of $C(x)$ can be obtained from the complex coefficients of eqns. 9 and 10 as follows:

$$c_i = d_i - e_{(n/2)+i} \qquad i = 0, \ldots, \left(\frac{n}{2}\right) - 2 \quad (11)$$

$$c_{(n/2)-1} = d_{(n/2)-1} \quad (12)$$

$$c_i = d_i + e_{i-(n/2)} \qquad i = \frac{n}{2}, \ldots, n-2 \quad (13)$$

$$c_{n-1} = e_{(n/2)-1} \quad (14)$$

Example: Consider two eight-point sequences $A = (a_0, \ldots, a_7) = (5, 2, 6, 9, 3, 4, 1, 10)$ and $B = (b_0, \ldots, b_7) = (4, 10, 2, 8, 5, 7, 6, 3)$ and consider the computation of their skew cyclic convolution $C = (c_0, \ldots, c_7)$ with arithmetic performed modulo 17. The traditional way of computing it (based on eqn. 6), requires $8^2 = 64$ multiplications and the result is $C = (c_0, \ldots, c_7) = (-234, -83, -104, 50, 67, 94, 166, 196)$, and by evaluating each c_i modulo 17 we obtain $C = (c_0, \ldots, c_7) = (4, 2, 15, 16, 16, 9, 13, 9)$. On the other hand, the same task can be computed using the QRNS with only 32 multiplications in the QRNS domain. Because 17 is prime and $17 = 4 \times 4 + 1$, then according to theorem 1, $x^2 + 1 = 0$ is solvable in Z_{17} and the QRNS mapping exists, and $\hat{j} = 4$ is one root of $x^2 + 1 = 0$ in Z_{17}; $(\langle 4^2 + 1 \rangle_{17} = 0)$. Following the notation of eqns. 7 and 8, the sequences A and B can be written as

$$(a_0, a_4)(a_1, a_5)(a_2, a_6)(a_3, a_7) = (5, 3)(2, 4)(6, 1)(9, 10)$$

$$(b_0, b_4)(b_1, b_5)(b_2, b_6)(b_3, b_7) = (4, 5)(10, 7)(2, 6)(8, 3)$$

where (a, b) denotes the complex number $a + jb$. Mapping in the QRNS domain the above complex numbers and multiplying the mapped sequences in a polynomial fashion in Z_{17}, we obtain

	(0, 10)	(1, 3)	(10, 2)	(15, 3)			
x)	(7, 1)	(4, 16)	(9, 12)	(3, 13)			
	(0, 10)	(7, 3)	(2, 2)	(3, 3)			
		(0, 7)	(4, 14)	(6, 15)	(9, 14)		
			(0, 1)	(9, 2)	(5, 7)	(16, 2)	
				(0, 11)	(3, 5)	(13, 9)	(11, 5)
+)	(0, 10)	(7, 10)	(6, 0)	(1, 14)	(0, 9)	(12, 11)	(11, 5)

Performing the inverse QRNS mapping of eqn. 5 on the above result and considering that $\langle 2^{-1} \rangle_{17} = 9$ and $\langle \hat{j}^{-1} \rangle_{17} = \langle 4^{-1} \rangle_{17} = 13$, we obtain $(t_0, t_1, \ldots, t_6) = [(d_0, e_0), (d_1, e_1), \ldots, (d_6, e_6)] = [(5, 3), (0, 6), (3, 5), (16, 9), (13, 1), (3, 15), (8, 5)]$. Using eqns. 11–14 we obtain $c = (c_0, c_1, \ldots, c_7) = (\langle 5 - 1 \rangle_{17}, \langle 0 - 15 \rangle_{17}, \langle 3 - 5 \rangle_{17}, 16, \langle 13 + 3 \rangle_{17}, \langle 3 + 6 \rangle_{17}, \langle 8 + 5 \rangle_{17}, 9) = (4, 2, 15, 16, 16, 9, 13, 9)$ and the result is correct.

Conclusion: The skew cyclic convolution of two n-point sequences can be computed as an $n \times n$ polynomial product requiring n^2 real multiplications. Alternatively, we have expressed the skew cyclic convolution as an $n/2 \times n/2$ product of two polynomials with complex coefficients requiring $n^2/4$ complex multiplications. We then applied the QRNS, which performs a complex product with only two real multiplications, to obtain the desired skew cyclic convolution with only $n^2/2$ real multiplications instead of n^2.

Acknowledgments: This work has been supported under NSF Grant No. CCR8910187.

A. SKAVANTZOS

Department of Electrical and Computer Engineering
Louisiana State University
Baton Rouge, LA 70803, USA

11th July 1991

References

1 TAYLOR, F. J.: 'Residue arithmetic: a tutorial with examples', *IEEE Computer*, 1984, **17**, (5), pp. 50–62
2 KROGMEIER, J. V., and JENKINS, W. K.: 'Error detection and correction in quadratic residue number systems'. Proc. 26th Midwest Symp. on Circuits and Systems, Puebla, MX, 1983, pp. 408–411
3 TAYLOR, F. J., PAPADOURAKIS, G., SKAVANTZOS, A., and STOURAITIS, A.: 'A radix-4 FFT using complex RNS arithmetic', *IEEE Trans.*, 1985, **C-34**, (6), pp. 573–576
4 SODERSTRAND, M. A., and POE, G. D.: 'Applications of quadratic like complex residue number system arithmetic to ultrasonics'. Proc. IEEE Int. Conf. on Acoustics, Speech and Signal Processing, San Diego, CA, March 1984, pp. 28A.5.1–28A.5.4
5 KRISHNAN, R., JULLIEN, G. A., and MILLER, W. C.: 'The modified quadratic residue number system (MQRNS) for complex high-speed signal processing', *IEEE Trans.*, 1986, **CAS-33**, (3), pp. 325–327

COMPLEMENTARY VERTICAL BIPOLAR TRANSISTOR PROCESS USING HIGH-ENERGY ION IMPLANTATION

Indexing terms: Transistors, Semiconductor devices and materials, Ion implantation

High-energy ion implantation is used as a key processing step in the formation of a complementary bipolar process with both transistor types being vertical. Both *npn* and *pnp* transistors are made vertically with a deep implanted collector region. Combinations of epitaxial and buried layers are avoided. Both transistors have an ideal Gummel plot with a current gain of about 60. Cutoff frequencies of over 1 GHz have been measured, which is much higher than for conventional lateral *pnp* transistors.

In contrast to MOS technology, complementary bipolar technology is unusual. Complementary bipolar circuits with a high performance *pnp* in the signal path offer the opportunity for designing push–pull circuits for both analogue[1] and digital applications.[2] In general complementary circuits lead to a reduction in power dissipation, increased switching speed and more flexible circuit design. Full benefits of these circuits can only be achieved if the performance of both transistors is similar.[3] In standard buried collector processes the lateral *pnp* is created without additional processing steps by using the *npn*-base diffusion as emitter and collector regions for the *pnp* and the epitaxial layer as *pnp* base.[4] The inferior performance of the lateral *pnp* transistor makes this device less suitable for signal processing and so the *pnp*s are only used as load devices. Complementary processes with both *npn* and *pnp* transistors realised vertically require additional processing steps. The processes proposed in the past exhibit an additional *p*-type buried layer and/or a second epitaxial layer.[5–8] We present a complementary vertical bipolar process, referred to as COVER, and demonstrate the feasibility of high-energy ion implantation as a processing step to create the collector regions of both *npn* and *pnp* transistors. Schematic cross-sections of the *npn* and *pnp* device structures, realised in the COVER process, are presented in Fig. 1. The planarisation layer and metallisation have not yet been included. A characteristic of this process is the realisation of the collector regions by high-energy ion implantation. Accordingly, no epitaxial and buried layers are necessary. To isolate both transistor types from the substrate, one of the transistor types is embedded in an additional implanted well. The option, whether the *npn* or the *pnp* transistor is isolated by an additional implanted well, is determined by the projected range of the dopants. Triply charged phosphorus ions with a maximum effective energy of 1·5 MeV are available in our implantation equipment. For boron the maximum effective energy is limited to 1 MeV, because triply charged boron ions are not available in the ion source of the implanter. Nevertheless, the largest

available depth for both transistors is obtained by using a 1 MeV boron doped well to isolate the *npn* transistor from the substrate, because the projected range of 1 MeV boron ions is

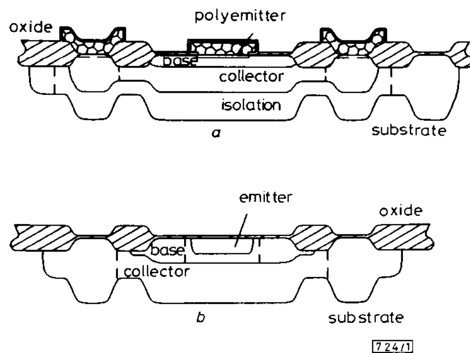

Fig. 1 *Schematic cross-sections of npn and pnp transistors*
——— junctions
▨ areas with different doping profile, although not separated by junction
a npn
b pnp

larger than that of the 1·5 MeV phosphorus ions, 1·73 μm as against 1·46 μm. As a consequence the substrate has to be *n*-type.

After LOCOS formation, the collector region of the *pnp* and the isolation well of the *npn* device are implanted simultaneously. In this way no additional mask is necessary for the isolation of the *npn* transistors. This *p*-type region is created by implantation of double charged boron ions with the maximum available energy of 500 keV and dose of $3 \times 10^{13}\,\mathrm{cm}^{-2}$. To complete the *pnp* transistor, a 500 keV phosphorus implantation with dose $10^{13}\,\mathrm{cm}^{-2}$ is used for the base region and a high dose boron implantation with an energy of 40 keV forms the emitter. The *npn* collector is created by a deep phosphorous implantation with an energy of 1 MeV. After boron is implanted with 40 keV at a dose of $1 \cdot 5 \times 10^{15}\,\mathrm{cm}^{-2}$ to form the *npn* base, the 300 nm thick polysilicon emitter is deposited and implanted with arsenic ($100\,\mathrm{keV}/4 \times 10^{15}\,\mathrm{cm}^{-2}$) to complete the *npn* transistor.

Photoresist is employed as masking material during the implantation steps. A 3 μm thick photoresist layer is adequate to prevent the high-energy implanted species from penetration into the underlying material. During the high-energy implantations the ion current is kept below $1\,\mu\mathrm{A/cm}^2$ to prevent the photoresist from cracking.

All implantations forming junctions were annealed immediately after implantation. To remove the implantation damage, a two-stage furnace anneal is performed at 600°C and 800°C each for 30 min in an N_2 ambient. During the first stage, the major crystal damage is removed and activation of the dopants, introduced during low-noise implantations, is achieved in the second stage.[9] This anneal sequence prevents the implanted species from fast diffusion during subsequent temperature treatments at higher temperatures,[10] such as the oxidation of the polysilicon emitter. The dopants, implanted at high dose, are activated during these high temperature steps. Fig. 2 shows the net doping profiles of the *npn* and *pnp* transistors, obtained by SIMS, together with the simulated profile. The measured profiles are consistent with the simulated profiles. The typical arsenic peak caused by segregation at the polysilicon–monosilicon interface is obvious in Fig. 2*a*.

In transistors with a buried and epitaxial layer, the doping concentrations of the epitaxial and buried layer can actually be set independently. The buried layer provides a low-ohmic collector region and the application of an epitaxial layer ensures a low base–collector capacitance C_{BC}, a high Early voltage V_A and a high base–collector breakdown voltage. In transistors with a high-energy ion implanted collector the collector concentration at the base–collector junction cannot be set independently of the maximum collector concentration. Hence, the Early voltage and base–collector breakdown voltage V_{BC_0} cannot be optimised separately from the collector resistance R_c. Therefore conflicting demands with respect to the collector implantation dose arise.*

Measured Gummel plots of both transistor types, shown in Fig. 3, exhibit ideal current characteristics, for collector and for base currents. The nearly ideal base current at low current levels indicates a minor influence of recombination in the

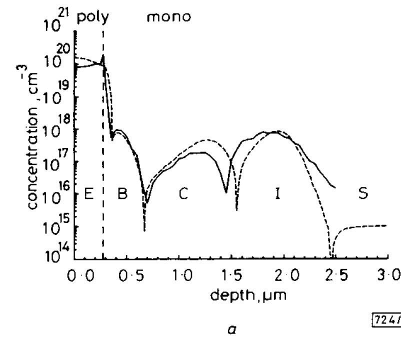

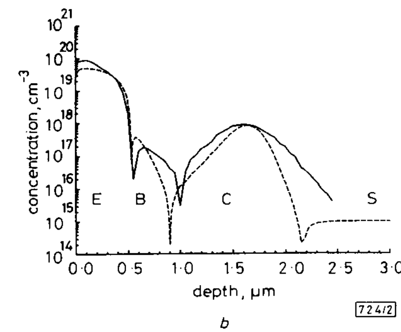

Fig. 2 *SIMS profiles of npn and pnp transistor, compared with SUPREMIII simulations*
a npn
b pnp
——— SIMS
- - - - SUPREM

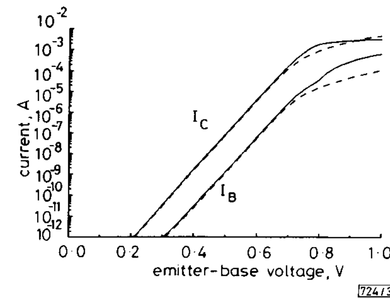

Fig. 3 *Gummel characteristic of npn and pnp transistor with emitter area of 10 × 40 μm*

* RAGAY, F. W., and WIJBURG, R. C. M.: 'Optimization of high-energy ion implanted collector regions for advanced bipolar transistors', submitted to 1991 Int. Semiconductor Devices Research Symp.

emitter–base depletion region. The low collector leakage currents demonstrate that no significant implantation damage in the base–collector depletion region is present. The current

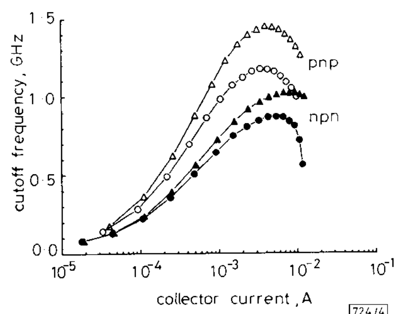

Fig. 4 *Cutoff frequency of npn and pnp transistor against collector current at V_{BC} = 1·5 and 3 V*

△, ○ *pnp*
▲, ● *npn*

gain for both transistors is about 60 and nearly constant over about six decades of current.

Initially the cutoff frequency (Fig. 4) rises with the collector current, but is limited by a constant delay time τ and reaches a maximum. Owing to the relatively high R_C of 210 and 175 Ω, respectively, for the *npn* and *pnp* transistors, the collector–base junction charging time $R_C \times C_{BC}$ is the major limitation of the maximum cutoff frequency and reduces at higher collector–base voltages V_{BC} due to the lower C_{BC}. For these transistors with a two-sided collector contact maximum cutoff frequencies of 1 GHz (*npn*) and 1·45 GHz (*pnp*) have been measured at V_{BC} = 3 V. The minimum delay times are primarily determined by $R_C \times C_{BC}$, 150 and 100 ps for the *npn* and *pnp* transistors, respectively, which is about a factor 4 larger than the transist time of the 0·25 μm wide base region. The cutoff frequency can be increased by a reduction of R_C. Unfortunately other device parameters suffer from a higher collector implantation dose.[11]

The maximum supply voltage of a complementary circuit is limited by the emitter–collector breakdown of the *npn* transistor. The $V_{ECo,\,npn}$ of 5·5 V is only half of $V_{ECo,\,pnp}$, due to the higher impact ionisation coefficients for electrons.[8]

The device performance is mainly limited by the collector implantation and will be substantially improved if 1·5 MeV implantations become available.

We conclude that high-energy ion implantation is a feasible technique for a complementary bipolar process with both *npn* and *pnp* transistors vertical. The process complexity is reduced essentially by the replacement of the buried and epitaxial layer with deep implanted layers to fabricate the collector regions. The device performance is restricted by the collector implantation and can be significantly improved by using 1·5 MeV implantations. Both transistors have a current gain of about 60, which is nearly constant over about six decades. Both *npn* and *pnp* transistors show ideal Gummel characteristics, indicating no effect of residual implantation damage.

The measured cutoff frequencies are over 1 GHz. The increase in performance of the all-implanted vertical *pnp* transistor is very striking compared with the conventionally used lateral *pnp* transistor.

In contrast to conventional buried layer processes the collector concentration at the base–collector junction cannot be set independently of the maximum collector concentration, for a deep implanted collector region. Optimising the device parameters leads to conflicting demands. For the *npn* transistor the emitter–collector breakdown voltage suffers most in the transistor design. This voltage cannot be increased without an intolerable rise in the collector resistance.

Acknowledgments: This Letter is dedicated to the memory of Prof. Middelhoek, who initiated the research on this subject. We thank K. Lippe and H. van der Vlist for their assistance during measurements. This work is financially supported by the Dutch Foundation for Fundamental Research (FOM).

F. W. RAGAY*
A. A. I. AARNINK
H. WALLINGA

MESA Research Institute
University of Twente
PO Box 217
7500 AE Enschede, The Netherlands

2nd September 1991

* Present address: Department of Applied Physics, Eindhoven University of Technology, PO Box 513, 5600 MB Eindhoven, The Netherlands

References

1 HUIJSING, J. H.: 'Integrated circuits for accurate linear analogue electric signal processing'. PhD Thesis, Technical University of Delft, 1981
2 WIEDMANN, S.: 'Potential of bipolar complementary device/circuit technology'. IEDM, 1987, pp. 96–99
3 NING, T. H., and TANG, D. D.: 'Bipolar trends', *Proc. IEEE*, 1986, **74**, pp. 1669–1677
4 AGRAZ-GUERENA, J., PANOUSIS, P. T., and MORRIS, B. L.: 'OXIL, a versatile bipolar VLSI technology', *IEEE Trans.*, 1980, **ED-27**, pp. 1397–1401
5 YAMAGUCHI, C., KOBAYASHI, Y., and SAKAI, T.: 'A 7 GHz pnp transistor for comlementary bipolar LSI'. Symp. VLSI Technology, 1987, pp. 39–40
6 INOUE, M., MATSUZAKAWA, A., KANDA, A., and SADAMATSU, H.: 'Self-aligned complementary bipolar transistors fabricated with a selective-oxidation mask', *IEEE Trans.*, 1987, **ED-34**, pp. 2146–2152
7 KIKKAWA, T., SUGANUMA, T., TANAKA, K., and HARA, T.: 'A new complementary transistor structure for analog integrated circuits'. IEDM Tech. Dig., 1980, pp. 65–68
8 SU, S. C., and MEINDL, J. D.: 'A new complementary bipolar transistor structure', *IEEE J. Solid-State Circuits*, 1972, **SC-7**, pp. 351–356
9 OOSTERHOFF, S., and MIDDELHOEK, J.: 'The annealing of 1 MeV implantations of boron in silicon', *Solid-State Electron.*, 1985, **28**, pp. 427–433
10 HOFKER, W. K., WERNER, H. W., OOSTHOEK, D. P., and DE GREFTE, H. A. M.: 'Influence of annealing on the concentration profiles of boron implantations in silicon', *Appl. Phys.*, 1973, **2**, pp. 265–278

Er^{3+}-DOPED MULTICOMPONENT GLASS CORE FIBRE AMPLIFIER PUMPED AT 1·48 μm

Indexing terms: Amplifiers, Optical fibres, Optics

An excellent fibre amplifier of Er^{3+}-doped silica fibre with a multicomponent core composed of Na_2O, CaO, Al_2O_3, SiO_2, and Er^{3+}, is realised. A maximum signal gain of 37 dB for a pump power of 23 mW at 1·48 μm and the gain coefficient of 3·5 dB/mW are attained.

Introduction: Much effort has been concentrated on realising an optical transmission system using Er^{3+}-doped fibre amplifiers.[1] The Er^{3+}-doped fibre amplifier has many advantages such as high gain, wide bandwidth, low noise, and polarisation independence. To employ an optical fibre amplifier as an optical component, it is necessary to broaden the signal gain bandwidth for a low pump power. At present, various host glasses are being investigated with the aim of amplifying the signal in the wide wavelength range. In particular, a gain of 25 dB and a 3 dB bandwidth of 35 nm have been obtained in Er^{3+}-doped silica fibre with SiO_2–Al_2O_3–P_2O_5 core.[2] Moreover, it has been reported that Er^{3+}-doped fluorozirconate glass fibre and multicomponent glass fibre have broader signal gain bandwidths and permit a higher Er^{3+} doping concentration.[3–5] As a result, Er^{3+}-doped silica fibre with CaO–Al_2O_3